A Rechargeable Na/Cl Battery

Hongjie Dai (hdai@stanford.edu)
Stanford University https://orcid.org/0000-0002-4906-4502

Guanzhou Zhu
Department of Chemistry and Bio-X, Stanford University

Xin Tian
Department of Chemistry and Bio-X, Stanford University

Hung-Chun Tai
Department of Chemical Engineering, National Chung Cheng University

Yuan-Yao Li
Department of Chemical Engineering, National Chung Cheng University

Jiachen Li
Department of Chemistry and Bio-X, Stanford University

Hao Sun
Department of Chemistry and Bio-X, Stanford University

Peng Liang
Department of Chemistry and Bio-X, Stanford University

Michael Angell
Stanford University

Cheng-Liang Huang
Department of Chemical Engineering, National Chung Cheng University

Ching-Shun Ku
National Synchrotron Radiation Research Center, Hsinchu 30076, Taiwan

Wei-Hsuan Hung
Institute of Materials Science and Engineering, National Central University

Jiang Shi Kai
Department of Chemical Engineering, National Taiwan University of Science and Technology

Yongtao Meng
Department of Chemistry and Bio-X, Stanford University

Bing Joe Hwang
National Taiwan University of Science and Technology https://orcid.org/0000-0002-3873-2149

Physical Sciences - Article

Keywords: rechargeable battery, sodium ion battery, Na anode, high capacity

Posted Date: October 1st, 2020

DOI: https://doi.org/10.21203/rs.3.rs-82836/v1

Version of Record: A version of this preprint was published at Nature on August 25th, 2021. See the published version at https://doi.org/10.1038/s41586-021-03757-z.

Abstract

Sodium is a promising anode material for batteries due to its low standard electrode potential, high abundance and low cost. In this work, we report a new rechargeable ~ 3.5 V sodium ion battery using Na anode, amorphous carbon-nanosphere cathode and a starting electrolyte comprised of $AlCl_3$ in $SOCl_2$ with fluoride-based additives. The battery, exhibiting ultrahigh ~ 2800 mAh/g first discharge capacity, could cycle with a high reversible capacity up to ~ 1000 mAh/g. Through battery cycling, the electrolyte evolved to contain NaCl, various sulfur and chlorine species that supported anode's Na/Na^+ redox and cathode's chloride/chlorine redox. Fluoride-rich additives were important in forming a solid-electrolyte interface, affording reversibility of the Na anode for a new class of high capacity secondary Na battery.

Main Text

Devising new battery concepts is important to meeting society's growing demand of energy storage. Different rechargeable batteries have been developed, including lithium ion batteries (LIBs), sodium ion batteries (SIBs) and aluminum ion batteries (AIBs)[1-9]. Prior to the invention of secondary LIBs, a primary Li-metal battery was developed in the 1970's using thionyl chloride ($SOCl_2$) as a catholyte, Li metal as anode and amorphous carbon as the positive electrode[10-16]. The Li-$SOCl_2$ battery was attractive due to its high energy density, but did not receive sustained interest due to the lack of rechargeability[17,18]. The battery discharges through Li anode oxidation and catholyte $SOCl_2$ reduction into sulfur (S), sulfur dioxide (SO_2), and chloride ion (Cl^-) on the carbon electrode[19,20]. The Cl^- ions react with Li^+ stripped from the Li anode to form LiCl deposited on the carbon surface until full coverage/passivation. This primary battery could deliver a high specific capacity of ~ 2300 mAh/g and high energy density of up to 710 mWh/g in a single discharge[19,20]. In addition, the Li-$SOCl_2$ batteries exhibit a long shelf life (10 – 20 years) and wide operation temperature range, and have been used in applications for the military, utility metering, GPS tracking and professional electronics[21,22].

Sodium batteries have also been actively pursued as an alternative to lithium due to its low standard electrode potential (only ~ 0.34 V higher than lithium), much lower price and equal promise for high energy density batteries[23,24]. Interestingly, there has been no report of sodium/$SOCl_2$ primary battery as in the lithium primary battery case, let alone rechargeable Na batteries in $SOCl_2$ based electrolyte.

Here, we report a sodium – amorphous carbon nanosphere (aCNS) battery with $AlCl_3$ and thionyl chloride as the main components in the starting electrolyte. The positive electrode contained a packed layer of ~ 60 nm high temperature CO_2 activated aCNS with an ultra-high surface area of 3000 – 3200 m^2/g. The battery delivered a high first discharge capacity ~ 2800 mAh/g (based on the mass of aCNS) with an average discharge voltage of ~ 3.2 V. To our surprise the battery could be cycled reversibly at a specific capacity up to 1000 mAh/g with a discharge voltage of ~ 3.55 V and an average coulombic efficiency ~ 99.5%. It was found that the first discharge of battery involved thionyl chloride ($SOCl_2$) catholyte

reduction to sulfur (S), sulfur dioxide (SO_2) and NaCl, with both NaCl and S deposited to passivate the positive aCNS electrode. When the battery was recharged, Cl^- in NaCl and $SOCl_2$ were oxidized to form Cl_2, SCl_2, S_2Cl_2, and SO_2Cl_2 in the system. Upon subsequent discharge, the dominant reaction was the reduction of Cl_2 to form NaCl, accompanied by SCl_2, S_2Cl_2 and SO_2Cl_2 reduction and $SOCl_2$ regeneration to complete the cycle. The Na/Cl secondary battery opens new possibilities for energy storage.

The amorphous carbon nanospheres were synthesized using a slightly modified Stöber method by first dissolving a triblock copolymer (F – 127), ammonia, resorcinol and formaldehyde in a mixture of deionized water and ethanol[25]. Upon centrifugation, the collected solid was dried and carbonized by heating at 800 ^oC for 4 hours in a nitrogen (N_2) environment followed by 1000 ºC for 45 minutes in carbon dioxide (CO_2) (see Methods). Scanning electron microscope (SEM) imaging showed that aCNS was made of closely packed ~ 60 nm carbon nanospheres (Fig. 1a). Transmission electron microscopy (TEM) showed amorphous carbon without lattice fringes, consistent with X-ray diffraction (XRD) data lacking well-defined diffraction peaks (Fig. 1b, Extended Data Fig. 1a, b). The Brunauer – Emmett – Teller theory (BET) surface area measurement indicated that aCNS had an impressive surface area between 3000 – 3200 m^2/g and high pore volume of 2.76 cm^3/g (Extended Data Table 1).

A Na/Cl battery was made by using sodium metal as the negative electrode and packed carbon nanosphere (aCNS) with PTFE binder in a Ni foam as the positive electrode in coin cell configuration (see Methods, Extended Data Fig. 2). The starting electrolyte was 4 M aluminum chloride ($AlCl_3$) dissolved in $SOCl_2$ with a mixture of 2 wt% sodium trifluoromethanesulfonimide (NaTFSI) and 2 wt% sodium bis(fluorosulfonyl)imide (NaFSI) as additives (Fig. 1a). The as-made battery was first discharged to 2 V, exhibiting a high capacity of ~ 2810 mAh/g with two obvious plateaus at ~ 3.47 V and 3.27 V (Fig. 1c). In the beginning of the discharge, the electrolyte was highly acidic with 4 M $AlCl_3$ and the plateau at ~ 3.47 V was attributed to Na oxidation, with the NaCl formed reacting with $AlCl_3$ to neutralize the electrolyte,

$$4\ Na + 4\ AlCl_3 + 2\ SOCl_2 \rightarrow 4\ NaAlCl_4 + S + SO_2 \quad (1)$$

As discharge progressed in a neutralized electrolyte, a lower discharge plateau of ~ 3.27 V appeared, corresponding to

$$4\ Na + 2\ SOCl_2 \rightarrow 4\ NaCl + S + SO_2 \quad (2)$$

with the NaCl product depositing onto the positive electrode and passivating the electrode. Similar two-plateau discharge was observed in Li/$SOCl_2$ cells in initially acidic electrolytes[11,17].

At the end of the first discharge sulfur dioxide (SO_2) formation was confirmed by mass-spectroscopy measurements of species inside the battery cell (Fig. 1d). Since SO_2 had a solubility of 2.47 M in $SOCl_2$ near room temperature at 22.3 ^oC and the molarity of SO_2 after the first discharge was ~ 1.34 M, most of

the SO_2 was dissolved in the electrolyte without increasing the pressure in the battery[26]. XRD and SEM imaging showed a thick layer of NaCl on the surface of the aCNS positive electrode (Fig. 1e), accompanied by a large increase in the electrochemical impedance of the battery (Extended Data Fig. 3a), consistent with passivation of the carbon electrode by deposited NaCl. The reduction chemistry of $SOCl_2$ to form S, SO_2 and Cl^- was similar to that in Li/$SOCl_2$ primary cells[17]. The proposed reactions (1) and (2) were supported by the fact that when an initially neutral electrolyte of 4 M NaCl + 4 M $AlCl_3$ in $SOCl_2$ was used, the higher plateau at ~ 3.47 V was not observed in the first discharge and only the plateau at ~ 3.25 V appeared throughout the whole discharge (Extended Data Fig. 3b).

When re-charging the battery after the first discharge, Na was deposited on the Na electrode and Cl^- from the deposited NaCl on the aCNS electrode was oxidized (at ~ 3.83 V, Fig. 2a) to form Cl_2 likely trapped in the abundant pores of aCNS (Extended Data Table 1). Oxidation of NaCl was probed by XPS showing that under increasing charging the percentage of NaCl on aCNS decreased, the NaCl crystallites on aCNS disappeared (revealed by SEM, Fig. 2b), and the XRD peaks of NaCl on aCNS decreased (Fig. 2c). In the beginning of charging, the voltage immediately spiked to ~ 4.16 V and then decreased to ~ 3.83 V. The voltage spike was observed in the beginning of charging in every cycle and was attributed to a high impedance caused by the NaCl coating layer on the aCNS electrode. Towards the end of charging (Fig. 2a), a slightly higher charging voltage plateau (~ 3.91 V) was observed and the reaction was attributed to the oxidation of $SOCl_2$ with formation of SCl_2, S_2Cl_2 and SO_2Cl_2 [18,27,28]. SO_2Cl_2 could also form by chemical reaction between Cl_2 generated through the main charging plateau and SO_2 generated in the first discharge step (Fig. 1d).

Using mass-spectroscopy (MS) we analyzed the speciation and composition of molecules in batteries by opening them in charged and discharged state (see Text S1 in SI: Mass Spectroscopy Analysis of Chemical Compositions in Na/Cl Battery Cells). The batteries were stopped at the 21st cycle running at a stable coulombic efficiency (CE) ~ 100% and opened. The main discharge plateau of ~ 3.55 V was found to be due to Cl_2 reduction, based on that the detected Cl_2 species (excluding fragments from other molecules, see Extended Data Figure 4) decreased to ~ 0 in fully discharged state from ~ 100 % in fully charged state (see Text S1). Reduction of molecular Cl_2 species generated and trapped in the pores of aCNS contributed to the majority of the discharge capacity of the battery during stable cycling. The main battery reaction responsible for the main charge/discharge plateaus during cycling was Na + ½ Cl_2 $\rightleftharpoons$ NaCl.

The two small discharge plateaus at ~ 3.69 V and ~ 3.18 V were attributed to reduction of S_2Cl_2/SCl_2 (formed at the end of the charging plateau) and SO_2Cl_2 (formed at the end of the charging step) respectively (Fig. 2a), based on capacity retention and mass-spectrometry experiments. We observed that the main discharge plateau at ~ 3.55 V decreased in capacity while the lower discharge plateau at ~ 3.18 V extended as a battery was held at open-circuit in a charged state over longer times (up to 5 days) (Fig. 2d). Mass spectrometry showed that the detected Cl_2 in the battery decreased proportionally to the ~ 3.55 V plateau capacity, together with a decrease in SO_2 and increased SO_2Cl_2 and increased ~ 3.18 V SO_2Cl_2

discharge plateau (Fig. 2e, Fig. 2f, Extended Data Fig. 5). During long retention times, Cl_2 and SO_2 in the system slowly recombined to form SO_2Cl_2, leading to the observed decrease in the 3.55 V Cl_2 reduction plateau and increase in the SO_2Cl_2 discharge plateau of ~ 3.18 V (Fig. 2d). Although open circuit holding of battery for days would sacrifice the higher discharge plateau at ~ 3.55 V, battery capacity retention was ~ 99.9%, and the 3.55 V plateau was immediately restored in subsequent cycles and the battery could continue to cycle with excellent reversibility (Fig. 2g, Fig. 2h).

Mass spectrometry also revealed that SCl_2 in the battery increased when fully charged and decreased to ~ 0 when the battery was discharged (Extended Data Fig. 4, Text S1). This and the fact that SCl_2 and S_2Cl_2 were known to be generated from oxidation of $SOCl_2$ at a higher potential suggested that the small plateau in the beginning of the high discharge voltage of ~ 3.69 V (~ 20 mAh/g or 4% of total capacity) corresponded to SCl_2/S_2Cl_2 reduction [10,18,27,28].

The chemical compositions inside the Na/Cl battery evolved in charged and discharged state, but between cycles the composition was largely kept constant since the main redox reactions involving species of Cl_2, SCl_2, S_2Cl_2, $SOCl_2$ and SO_2Cl_2 were largely reversible. The reduction product of NaCl formed by discharge reacted with $AlCl_4^-$•$SOCl^+$ in the electrolyte to re-generate $SOCl_2$ oxidized in the charging step, which was important to rechargeability of the Na/Cl battery [18].

The Na/Cl battery cycled reversibly and stably for more than 100 cycles at a set specific capacity of 500 mAh/g at 150 mA/g current (Fig. 3a). The reversible battery capacity of the Na/Cl cell was found to be up to ~ 1000 mAh/g with the charge – discharge curve maintaining its overall shape as capacity varied from 375 mAh/g to 1000 mAh/g, with the main ~ 3.83 V charge and ~ 3.55 V discharge plateaus simply extended their length and capacity (Fig. 3b, Fig. 3d). The battery could cycle reversibly at various specific capacities and currents with no obvious decrease in coulombic efficiency (Fig. 3c). At lower currents the polarization voltage showed slight decreases (Fig. 3b, Fig. 3d). For a specific capacity of 1000 mAh/g, the energy density that the ~ 3.5 V Na/Cl battery could deliver was ~ 3.5 Wh/g (based on aCNS mass) with an impressive energy efficiency of 92.4%. Importantly, throughout cycling of all of our Na/Cl battery coin cells, we encountered no safety problems. We found no pressurizing problems due to strong solvation of SO_2, Cl_2 species by $SOCl_2$ SO_2Cl_2 and $NaAlCl_4$ in the electrolyte.

Since NaCl was the major species undergoing oxidation during charging, the upper limit of the charging capacity was set by the amount of NaCl deposited on the aCNS in the first discharge. During the first discharge, the high plateau at ~ 3.47 V produced NaCl reacting to neutralize the electrolyte (eq. 1). The lower plateau at ~ 3.27 V (~ 1400 mAh/g) led to the formation of NaCl deposits (eq. 2), which set an upper limit of the reversible Cl^-/Cl_2 capacity. We observed that the battery could cycle up to 1300 mAh/g close to the ~ 1400 mAh/g limit but with a poor cycle life likely caused by the reduced stability of the Na anode under higher charging conditions.

We found that the Na/Cl battery decay was due to the Na anode and not the cathode, based on that a battery using fresh Na, fresh electrolyte and a recycled aCNS electrode from a decayed battery could cycle stably again with normal charge – discharge behavior. The fluoride containing additives, known to facilitate the formation of robust solid electrolyte interphase (SEI) on alkaline metal battery anodes in general, were found important to prolong the cycle life of our Na/Cl battery[29-33]. Batteries with no additive showed the worst cycle life (< 50 cycles). When only 2 wt% NaFSI was added, the cycle life of the battery improved to about 70 cycles, and when a mixture of 2 wt% NaFSI/NaTFSI was added, the battery showed the best cycling performance (> 100 cycles) (Fig. 4a). The composition on Na metal surface after immersion in electrolyte (4 M $AlCl_3$ in $SOCl_2$) with and without 2 wt% NaFSI/NaTFSI additives were analyzed by XPS. We found NaCl coating on Na metal due to reaction with $SOCl_2$ in both samples, analogous to LiCl formed on Li in Li – $SOCl_2$ primary batteries (Extended Data Fig. S6a, d)[34-36]. Abundant elements of F, N and S, assigned to NaF, Na_2SO_4, $Na_2S_2O_3$, Na_2SO_3 were observed only on Na in the fluoride containing electrolyte, suggesting reactions between Na and anions FSI^- and $TFSI^-$ forming a more protective SEI layer on Na (Extended Data Fig. S6a, b, c)[37-40].

The fluoride containing SEI was formed in the first few cycles over which the coulombic efficiency gradually increased to ~ 100% (Fig. 3a). A more robust SEI layer could prevent or slow down reactions with corrosive species in the electrolyte including Cl_2, $SOCl_2$, SCl_2 and SO_2Cl_2. When the battery eventually decayed, the overpotential increased accompanied by a drop in coulombic efficiency (Extended Data Fig. 6e). The impedance of the battery increased significantly as well, caused by the build-up of thick insulating NaCl on the Na anode. Our observation was consistent with previous results that the SEI on alkaline metal anode was more robust when both FSI^- and $TFSI^-$ anions were present, leading to better sodium battery cycle lives[1,41].

Lastly, our amorphous carbon nanosphere was a novel positive electrode material for the Na/Cl battery owing to its ultra-high surface area (3000 – 3200 m^2/g) and high porosity (2.76 cm^3/g). We compared several widely used commercially available amorphous carbon including acetylene black (AB) and ketjenblack carbon black (KJ) to aCNS as positive electrode (Fig. 4b). The battery using AB as positive electrode could only run for less than 20 cycles and battery using KJ as positive electrode showed a better cycle life than AB but the coulombic efficiency was always lower than 90%. We attributed aCNS's high cycling performance to both high surface area and porosity that were superior to AB. On the other hand, KJ showed higher pore volume but exhibited much lower surface area than aCNS (Extended Data Table 1). High surface area and porosity helped the positive electrode to better accommodate insoluble discharge product, i.e., NaCl in our battery[42]. In addition, carbon with high surface area and porosity could trap the corrosive species such as Cl_2, SCl_2, SO_2Cl_2 in the electrolyte better, reducing corrosion of the anode and improving battery's cycle life.

We employed the Na/Cl battery to light up of an LED light that required an operating voltage of 3.0 V – 3.2 V. The current measured through the LED was ~ 12.03 mA with a high current density of 4.57 mA/cm^2 Na, equivalent to a discharge rate of 1563.35 mA/g (based on aCNS mass) (Fig. 4c). The new

rechargeable Na/Cl battery with ultra-high first discharge capacity and subsequent high reversible capacity gives a new life to decades old primary batteries. There is still room to further improve the battery performance. Novel electrolyte additives can be explored for more robust SEI to further prolong the battery cycle life. In addition, other positive electrode materials can also be investigated.

Data Availability the authors declare that the data supporting the findings of this study are available within the paper and its supplementary information files.

Methods

Synthesis of aCNS

50 mL of deionized water and 20 mL of ethanol (> 99.9 %, J. T. Baker) were mixed uniformly at room temperature. 0.25 g of triblock copolymer, F-127 (PEO106-PPO70-PEO106, MW: 14600, Aldrich), was then added in the mixture and stirred for about 10 minutes. After F-127 dissolved completely, 0.5 g of ammonia solution (25 %, Choneye, Taiwan) was then added in the solution and stirred for about 30 minutes followed by adding 0.5 g of resorcinol (99%, Alfa Aesar) into the solution. Finally, 0.763 g of formaldehyde solution (37 wt%, Aldrich) was added gradually into the solution and stirred for 24 hours at room temperature. The solution was centrifuged with 14,900 rpm to separate the solid and liquid. The solid was dried at 100 ^{o}C in oven and heated at 350 ^{o}C for 2 hours in N_2 to remove the template. The carbonization process was conducted at 800 ^{o}C for 4 hours in N_2 followed by the activation process using CO_2 at 1000 °C for 45 minutes.

Fabrication of aCNS electrode

90% by weight of aCNS and 10% by weight of polytetrafluoroethylene (60% aqueous PTFE dispersion, FuelCellStore) were mixed in 100% ethanol (Fisher Scientific). The mixture was sonicated for 2 hours until the aCNS was uniformly dispersed in ethanol. Ni foam substrate was cut into circular shape with diameter of 1.5 cm using a compact precision disc cutter (MTI, MSK-T-07). The circular Ni foam substrate was sonicated in 100% ethanol for 15 minutes and dried in an 80 ^{o}C oven until all the ethanol evaporated. The weight of the Ni foam substrate was measured and then placed to hover over a hot plate. The aCNS, PTFE and ethanol mixture was then slowly dropped (180 µL each time) onto the Ni foam. Between each drop, we waited for approximately 4 minutes to allow all the ethanol from previous drop to fully evaporate. This process was repeated and stopped until the loading of the aCNS on Ni foam substrate reached 4.5 – 5 mg/cm^2. The electrodes were then dried in an 80 ^{o}C oven overnight. After drying, the electrode was pressed using a spaghetti roller and the final weight of the electrode was measured. After calculating the weight of aCNS, i.e. final weight of the electrode minus initial weight of the Ni foam times 90%, the electrode was ready to be used in a battery.

Electrolyte making

The electrolyte was made inside an argon-filled glovebox. NaFSI (TCI Chemical) and NaTFSI (Alfa Aesar) were dried at 100 ^{o}C vacuum oven overnight before use and stored in an argon – filled glovebox. Thionyl chloride (purified, Spectrum catalog # TH138) was used without any further purification. The appropriate amount of thionyl chloride liquid was added into a 20 mL scintillation vial (Fisher Scientific) and its weight was measured. 4 M aluminum chloride (Fluka, 99%, anhydrous, granular) were weighed and added to the thionyl chloride and stirred until all the aluminum chloride was fully dissolved. Then the appropriate amount of NaFSI and NaTFSI (2 wt% of the total weight of aluminum chloride and thionyl chloride) were added to the solution and stirred until both NaFSI and NaTFSI completely dissolved, after which the electrolyte was ready to be used.

Battery making

All batteries were made inside an argon-filled glovebox. Sodium metal block (Sigma Aldrich) was dried using kimwipes (Kimberly – Clark Professional^{TM} Kimtech Science^{TM}) to remove the mineral oil on the surface. Razor blade was then used to cut all sides of the Na block to expose the shiny Na metal. The sodium metal block was then placed inside a zip lock bag and pressed using a scintillation vial to make thin sodium foil. The sodium foil was then pasted onto the spacer in a coin cell. Any extra sodium was removed so that the sodium foil had the exact shape as the spacer and could be used as the negative electrode. aCNS loaded on Ni foam was used as the positive electrode. 2 layers of quartz fiber filters (Sterlitech, Advantec, QR – 100) were used as the separators and were dried in 120 ^{o}C vacuum oven overnight before each use. The aCNS positive electrode was put in the middle of the SS316 positive coin cell case. 2 layers of QR – 100 separators were then put on top of the aCNS positive electrode. 150 µL of the electrolyte (4 M $AlCl_3$ in $SOCl_2$ + 2 wt% NaFSI + 2 wt% NaTFSI) were then added to wet the QR – 100 separators. The Na negative electrode on spacer was then put on top of the separators, with Na foil directly facing the aCNS positive electrode. One piece of spring was put on top of the spacer. Lastly, one layer of PTFE foil was put on top of the spring and underneath the SS316 negative coin cell case to prevent corrosion from the electrolyte. After all the components of the coin cell were put together, the coin cell was pressed using a digital pressure controlled electric crimper (MTI, MSK-160E) with the pressure reading set to 9.23. Then the coin cell was taken out the glovebox and was tested using a battery tester from Neware, BTS80, Version 17.

Electrochemical Impedance Spectroscopy

The electrochemical impedance spectroscopy (EIS) of the battery was measured using a potentiostat/galvanostat (model CHI 760D, CH Instruments). The working electrode was connected to the aCNS positive electrode, and the counter and reference electrodes were connected to the sodium negative electrode. The initial voltage of the measurement was set to be the open circuit potential of the battery at the time of the measurement. The high frequency was 1 10^5 Hz and the low frequency was 0.01 Hz. The amplitude of the measurement was 0.005 V.

Scanning Electron Microscope (SEM)

SEM imaging was measured using Hitachi/S-4800 SEM instrument. To conduct SEM imaging on aCNS, aCNS powder was first stuck on the sample stage of SEM using double-sided conductive carbon adhesive tapes and the stage was then loaded into the SEM chamber for measurement. To conduct SEM imaging on electrodes in actual battery, the battery was first opened inside an argon – filled glovebox. The electrodes were taken out from the opened battery and transferred into the argon – filled antechamber of the glovebox. The electrodes were vacuumed and dried inside the antechamber for approximately 3 hours to remove any electrolyte trapped in them. After drying, the electrodes were transferred back into the glovebox and ready to be characterized. The samples were stuck onto the SEM sample stage using double-sided conductive carbon adhesive tapes and introduced into the SEM chamber for measurement. The sample was observed by SEM with 15 kV acceleration voltage of an electron beam at a pressure of 10^{-7} torr. A magnification of 200,000 could be achieved.

Transmission Electron Microscopy (TEM)

Transmission electron microscopy (TEM) imaging was conducted on a FEI EO Tecnai F20 G2 MAT S-TWIN field transmission electron microscopy. To prepare samples for TEM imaging, 0.02 g aCNS was dispersed in 10 mL deionized water in a 20 mL scintillation vial (Fisher Scientific). The mixture was sonicated for 30 minutes until a uniform dispersion of aCNS was achieved. After sonication, one drop of the mixture was dropped onto a Cu TEM grid using glass dropping pipette. The grid was then placed inside a 100 ^{o}C oven for 3 days. After drying, the Cu TEM grid with aCNS sample was introduced into the TEM instrument operating at 200 kV for measurement.

XPS Experiments

XPS measurement was conducted in SNSF facility, Stanford University and the XPS instrument used was PHI VersProbe 1. To conduct XPS on sodium immersed in different solutions (4 M $AlCl_3$ + 2 wt% NaFSI/NaTFSI in $SOCl_2$ or 4 M $AlCl_3$ in $SOCl_2$), the sample preparation was done inside an argon – filled glovebox. Na foil was prepared the same way as preparing Na electrode in battery (Battery Making). After immersion in the appropriate solution for 1 hour, the Na foil was taken out from the solution and any liquid remaining on the surface was dried using kimwipes (Kimberly – Clark Professional^{TM} Kimtech Science^{TM}). The antechamber of the glovebox was refilled with argon and the sample was transferred into the antechamber, in which the sample was vacuumed dried. After drying, the sample was transferred into the glovebox and was ready to be characterized by XPS. To conduct XPS on electrodes from battery, the sample preparation was the same as the sample preparation for SEM imaging. After sample preparation, the sample was clamped onto the XPS stage and was transferred into the main chamber of the XPS instrument for measurement. All the spectra reported were the spectra obtained after 20 nm argon ion sputtering to remove any possible surface contamination during sample handling.

X – ray Diffraction

X-ray diffraction (XRD) was conducted on an X-ray diffraction system (Rigaku Miniflex 600 Benchtop) with Cu Kα radiation. The aCNS powder was put on the XRD sample stage and a razor blade was used to press the powder until a flat surface was obtained and the powder was uniformly and firmly distributed over the sample stage. Any extra powder was carefully removed from the sample stage. The sample stage was then transferred into the center of the XRD instrument for measurement. The start angle and the stop angle were set to be 5^o and 90^o, respectively, with the scan speed of 3^o/min. To conduct XRD measurements of electrodes from battery, the sample preparation was the same as the sample preparation for SEM imaging, and XRD was performed after the samples were transferred out from glovebox into the XRD instrument.

pH Measurements of Carbon

pH was measured by dissolving 1 g of the carbon into 30 mL deionized water. The solution was then transferred into a round bottom flask and boiled under reflux for 5 minutes. After 5 minutes of boiling, the round bottom flask was removed from the heat source and allowed to cool down to room temperature. After all the carbon particles has sunk to the bottom of the round bottom flask, the pH of the clear liquid at top was measured.

Brunauer – Emmett – Teller (BET) Surface Area and Porosity

Brunauer–Emmett–Teller (BET) surface area and pore volume were measured by an 2020 Accelerated Surface Area and Porosimetry System from Micromeritics. Before each measurement, the appropriate amount of carbon (~ 0.14 g) was weighed and placed in the instrument for degas at (350 ^{o}C). After degassing, the weight of the carbon was measured again and this weight was input into the software for final surface area and porosity analysis. In the final analysis, the evacuation time was set to be (6 hours) and dose amount was set to be (10 cm^3/g STP). After the measurement was done by the instrument, the surface area and porosity were reported.

Volatile Percent of Carbon

Volatile % was measured using a high gravimetric sensitivity thermogravimetric analysis (TGA) instrument. The initial weight of the carbon samples was measured before introducing the samples into the TGA instrument. Then the temperature of the instrument was increased to 80 ^{o}C in 5 minutes and held at 80 ^{o}C for 10 minutes. After the 10 minutes isothermal step, the temperature was increased to 160 ^{o}C in 8 minutes and then held at 160 ^{o}C for 10 minutes. The final weight of the carbon was measured and the volatile % of the carbon was equal to the percent difference between the initial weight and the final weight[43].

Declarations

Acknowledgments part of this work was performed at the Stanford Nano Shared Facilities (SNSF), supported by the National Science Foundation under award ECCS-1542152.

Author contributions G. Zhu and H. Dai. conceived the main idea of the project. G. Zhu and X. Tian performed the experiments and contributed equally to this work. G.Z. performed the mass spectroscopy measurement of species in the battery. H. –C. Tai, Z. –L. Huang and Y. –Y. Li prepared the aCNS raw material. H. –C. Tai performed the characterizations of aCNS (SEM, TEM, XRD etc.). J. Li, C. –S. Ku, W. -H. Hung, J. Kai and B. –J. Hwang performed characterizations of electrodes in battery. G. Zhu and H. Sun performed the LED demo of the Na/Cl battery. G. Zhu, P. Liang and M. Angell performed X-ray photoelectron spectroscopy measurements. G. Zhu and H. Dai. prepared the manuscript. All authors participated in experimental data/results analysis and discussion;

Competing interests Authors declare no competing interests.

Supplementary Information is available for this paper.

Correspondence and requests for materials should be addressed to H. Dai. (hdai1@stanford.edu).

References

1 Sun, H. *et al.* A safe and non-flammable sodium metal battery based on an ionic liquid electrolyte. *Nature Communications* 10, 3302, doi:10.1038/s41467-019-11102-2 (2019).

2 Angell, M., Zhu, G., Lin, M.-C., Rong, Y. & Dai, H. Ionic Liquid Analogs of AlCl3 with Urea Derivatives as Electrolytes for Aluminum Batteries. *Advanced Functional Materials* 30, 1901928, doi:10.1002/adfm.201901928 (2020).

3 Zhu, G. *et al.* Rechargeable aluminum batteries: effects of cations in ionic liquid electrolytes. *RSC Advances* 9, 11322-11330, doi:10.1039/C9RA00765B (2019).

4 Lin, M.-C. *et al.* An ultrafast rechargeable aluminium-ion battery. *Nature* 520, 324-328, doi:10.1038/nature14340

http://www.nature.com/nature/journal/v520/n7547/abs/nature14340.html#supplementary-information (2015).

5 Angell, M. *et al.* High Coulombic efficiency aluminum-ion battery using an AlCl3-urea ionic liquid analog electrolyte. *Proceedings of the National Academy of Sciences* 114, 834-839, doi:10.1073/pnas.1619795114 (2017).

6 Pan, C.-J. *et al.* An operando X-ray diffraction study of chloroaluminate anion-graphite intercalation in aluminum batteries. *Proceedings of the National Academy of Sciences* 115, 5670-5675, doi:10.1073/pnas.1803576115 (2018).

7 Di Lecce, D., Carbone, L., Gancitano, V. & Hassoun, J. Rechargeable lithium battery using non-flammable electrolyte based on tetraethylene glycol dimethyl ether and olivine cathodes. *Journal of*

Power Sources 334, 146-153, doi:https://doi.org/10.1016/j.jpowsour.2016.09.164 (2016).

8 Agostini, M., Xiong, S., Matic, A. & Hassoun, J. Polysulfide-containing Glyme-based Electrolytes for Lithium Sulfur Battery. *Chemistry of Materials* 27, 4604-4611, doi:10.1021/acs.chemmater.5b00896 (2015).

9 Cai, K., Song, M.-K., Cairns, E. J. & Zhang, Y. Nanostructured Li2S–C Composites as Cathode Material for High-Energy Lithium/Sulfur Batteries. *Nano Letters* 12, 6474-6479, doi:10.1021/nl303965a (2012).

10 Venkatasetty, H. V. & Saathoff, D. J. Properties of LiAlCl4 - SOCl2 Solutions for Li / SOCl2 Battery. *Journal of The Electrochemical Society* 128, 773-777, doi:10.1149/1.2127503 (1981).

11 Tsaur, K. C. & Pollard, R. Mathematical Modeling of the Lithium, Thionyl Chloride Static Cell: II . Acid Electrolyte. *Journal of The Electrochemical Society* 131, 984-990, doi:10.1149/1.2115788 (1984).

12 Istone, W. K. & Brodd, R. J. The Mechanisms of Thionyl Chloride Reduction at Solid Electrodes. *Journal of The Electrochemical Society* 131, 2467-2470, doi:10.1149/1.2115325 (1984).

13 Gangadharan, R., Namboodiri, P. N. N., Prasad, K. V. & Viswanathan, R. The lithium—thionyl chloride battery — a review. *Journal of Power Sources* 4, 1-9, doi:https://doi.org/10.1016/0378-7753(79)80032-4 (1979).

14 Madou, M. J. & Szpak, S. Investigation of SOCl2 Reduction by Cyclic Voltammetry and AC Impedance Measurements. *Journal of The Electrochemical Society* 131, 2471-2475, doi:10.1149/1.2115326 (1984).

15 Bedfer, Y., Corset, J., Dhamelincourt, M. C., Wallart, F. & Barbier, P. Raman spectroscopic studies of the structure of electrolytes used in the Li/SOCl2 battery. *Journal of Power Sources* 9, 267-272, doi:https://doi.org/10.1016/0378-7753(83)87027-X (1983).

16 Carter, B. J. *et al.* Mechanistic studies related to the safety of Li/SOCl/sub 2/ cells. *J. Electrochem. Soc.; (United States)*, Medium: X; Size: Pages: 525-528 (1985).

17 Klinedinst, K. A. & Domeniconi, M. J. High Rate Discharge Characteristics of Li / SOCl2 Cells. *Journal of The Electrochemical Society* 127, 539-544, doi:10.1149/1.2129708 (1980).

18 Abraham, K. M. & Mank, R. M. Some Chemistry in the Li / SOCl2 Cell. *Journal of The Electrochemical Society* 127, 2091-2096, doi:10.1149/1.2129352 (1980).

19 Wang, D. *et al.* The Effects of Pore Size on Electrical Performance in Lithium-Thionyl Chloride Batteries. *Frontiers in Materials* 6, doi:10.3389/fmats.2019.00245 (2019).

20 Marinčić, N. Materials balance in primary batteries. II. Lithium inorganic batteries at high discharge rates. *Journal of Applied Electrochemistry* 6, 51-58, doi:10.1007/BF01058870 (1976).

21 Spotnitz, R. M., Yeduvaka, G. S., Nagasubramanian, G. & Jungst, R. Modeling self-discharge of Li/SOCl2 cells. *Journal of Power Sources* 163, 578-583, doi:https://doi.org/10.1016/j.jpowsour.2006.09.025 (2006).

22 Morrison, M. M. & Marincic, N. Studies in lithium oxyhalide cells for downhole instrumentation Use of lithium tetrachlorogallate electrolyte in Li/SOCl2 cells. *Journal of Power Sources* 45, 343-352, doi:https://doi.org/10.1016/0378-7753(93)80023-I (1993).

23 Barpanda, P., Oyama, G., Nishimura, S.-i., Chung, S.-C. & Yamada, A. A 3.8-V earth-abundant sodium battery electrode. *Nature Communications* 5, 4358, doi:10.1038/ncomms5358 (2014).

24 Zhu, C., Kopold, P., van Aken, P. A., Maier, J. & Yu, Y. High Power–High Energy Sodium Battery Based on Threefold Interpenetrating Network. *Advanced Materials* 28, 2409-2416, doi:10.1002/adma.201505943 (2016).

25 Liu, J. *et al.* Extension of The Stöber Method to the Preparation of Monodisperse Resorcinol–Formaldehyde Resin Polymer and Carbon Spheres. *Angewandte Chemie International Edition* 50, 5947-5951, doi:10.1002/anie.201102011 (2011).

26 Klinedinst, K. A. & McLaughlin, M. L. Solubilities of sulfur and sulfur dioxide in thionyl chloride with and without 1.8 M lithium tetrachloroaluminate. *Journal of Chemical & Engineering Data* 24, 203-206, doi:10.1021/je60082a017 (1979).

27 Gross, S. & Society, E. *Proceedings of the Symposium on Battery Design and Optimization*. (Battery Division, Electrochemical Society, 1979).

28 Abraham, K. M., Mank, R. M. & Holleck, G. L. Investigations of the safety of Li/SOCl2 batteries. (1979).

29 Fujii, K. *et al.* Unusual Li+ Ion Solvation Structure in Bis(fluorosulfonyl)amide Based Ionic Liquid. *The Journal of Physical Chemistry C* 117, 19314-19324, doi:10.1021/jp4053264 (2013).

30 Takada, K. *et al.* Unusual Passivation Ability of Superconcentrated Electrolytes toward Hard Carbon Negative Electrodes in Sodium-Ion Batteries. *ACS Applied Materials & Interfaces* 9, 33802-33809, doi:10.1021/acsami.7b08414 (2017).

31 Matsumoto, K. *et al.* Thermal, Physical, and Electrochemical Properties of Li[N(SO2F)2]-[1-Ethyl-3-methylimidazolium][N(SO2F)2] Ionic Liquid Electrolytes for Li Secondary Batteries Operated at Room and Intermediate Temperatures. *The Journal of Physical Chemistry C* 121, 9209-9219, doi:10.1021/acs.jpcc.7b02296 (2017).

32 Lee, J. *et al.* Ultraconcentrated Sodium Bis(fluorosulfonyl)imide-Based Electrolytes for High-Performance Sodium Metal Batteries. *ACS Applied Materials & Interfaces* 9, 3723-3732, doi:10.1021/acsami.6b14878 (2017).

33 Sakaebe, H. & Matsumoto, H. N-Methyl-N-propylpiperidinium bis(trifluoromethanesulfonyl)imide (PP13–TFSI) – novel electrolyte base for Li battery. *Electrochemistry Communications* 5, 594-598, doi:https://doi.org/10.1016/S1388-2481(03)00137-1 (2003).

34 Dey, A. N. Lithium anode film and organic and inorganic electrolyte batteries. *Thin Solid Films* 43, 131-171, doi:https://doi.org/10.1016/0040-6090(77)90383-2 (1977).

35 Moshtev, R. V. The Primary Passive Film on Li in SOCl[sub 2] Electrolyte Solutions. *Journal of The Electrochemical Society* 128, 1851, doi:10.1149/1.2127750 (1981).

36 Fleischer, N. A., Manske, S. M. & Ekern, R. J. Reduction of Voltage Delay in the Li / SOCl2 System via Suitable Choice of Electrolyte Salts. *Journal of The Electrochemical Society* 131, 1733-1738, doi:10.1149/1.2115951 (1984).

37 Terlingen, J. G. A., Jan, F. & Hoffman, A. S. Immobilization of surface active compounds on polymer supports using a gas discharge process. *Journal of Biomaterials Science, Polymer Edition* 4, 31-33, doi:10.1163/156856292X00277 (1993).

38 Abraham, K. M. The Lithium Surface Film in the Li/SO[sub 2] Cell. *Journal of The Electrochemical Society* 133, 1307, doi:10.1149/1.2108858 (1986).

39 Siriwardane, R. V. & Cook, J. M. Interactions of SO2 with sodium deposited on CaO. *Journal of Colloid and Interface Science* 114, 525-535, doi:https://doi.org/10.1016/0021-9797(86)90438-8 (1986).

40 Peisert, H., Chassé, T., Streubel, P., Meisel, A. & Szargan, R. Relaxation energies in XPS and XAES of solid sulfur compounds. *Journal of Electron Spectroscopy and Related Phenomena* 68, 321-328, doi:https://doi.org/10.1016/0368-2048(94)02129-5 (1994).

41 Hosokawa, T. *et al.* Stability of Ionic Liquids against Sodium Metal: A Comparative Study of 1-Ethyl-3-methylimidazolium Ionic Liquids with Bis(fluorosulfonyl)amide and Bis(trifluoromethylsulfonyl)amide. *The Journal of Physical Chemistry C* 120, 9628-9636, doi:10.1021/acs.jpcc.6b02061 (2016).

42 Gilman, S. The Reduction of Sulfuryl Chloride at Teflon-Bonded Carbon Cathodes. *Journal of The Electrochemical Society* 127, 1427, doi:10.1149/1.2129924 (1980).

43 1998 - 2020 PerkinElmer Inc. Cassel, W. J. S. a. R. B. High Sensitivity Volatiles Analysis by TGA, http://www.perkinelmer.com/

Figures

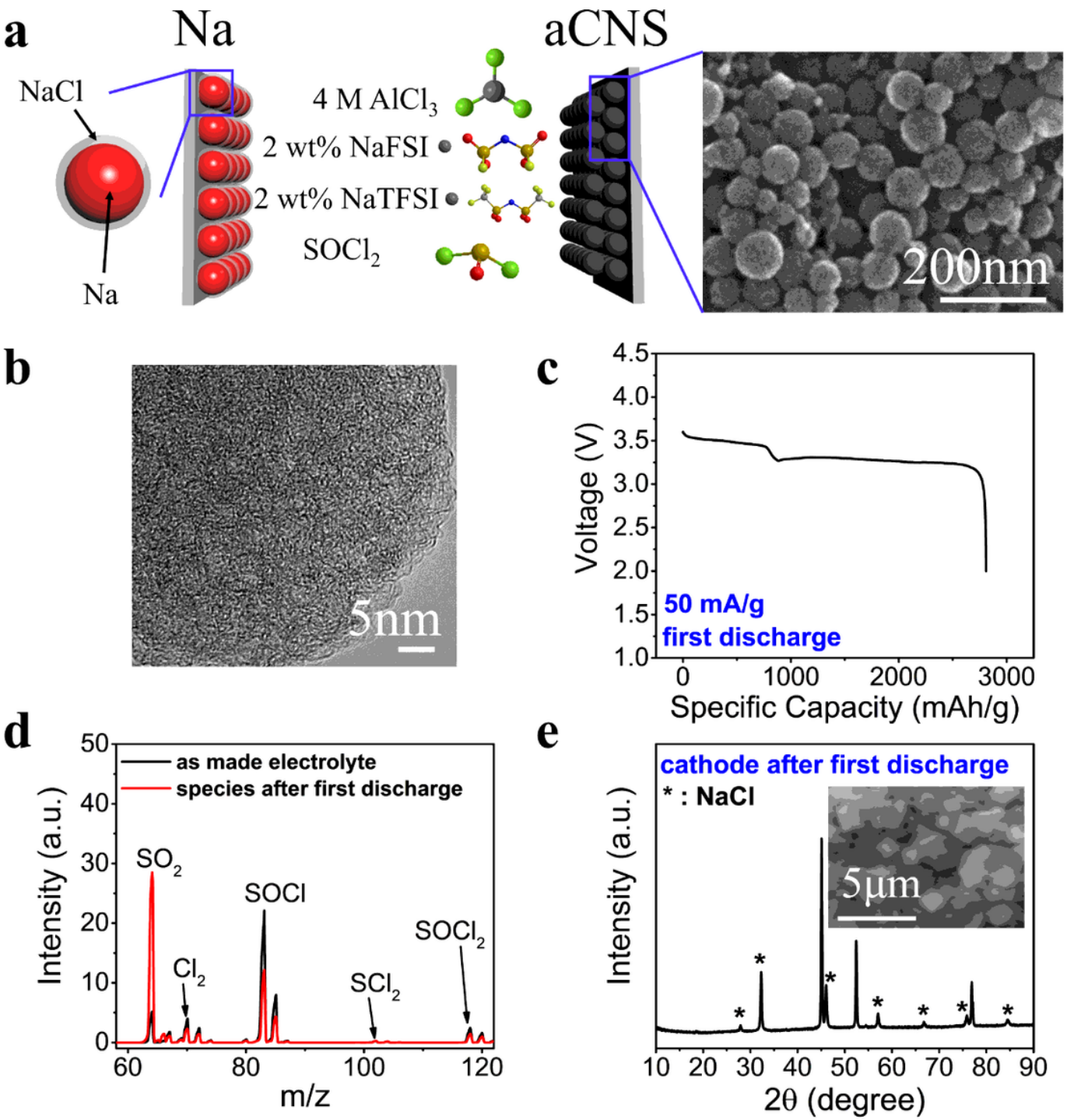

Figure 1

A high capacity Na/Cl battery through the first discharge. a, schematic drawing of the Na/Cl battery with initial electrolyte composition and SEM imaging of amorphous carbon nanosphere (aCNS) in the cathode. b, TEM imaging of aCNS. c, first discharge curve of the Na/Cl battery. d, Ar normalized mass spectroscopy data of as made electrolyte vs. species in an opened battery after first discharge. e, XRD

spectrum of aCNS after first discharge, unlabeled peaks were Ni current collector (inset: SEM imaging of aCNS after first discharge).

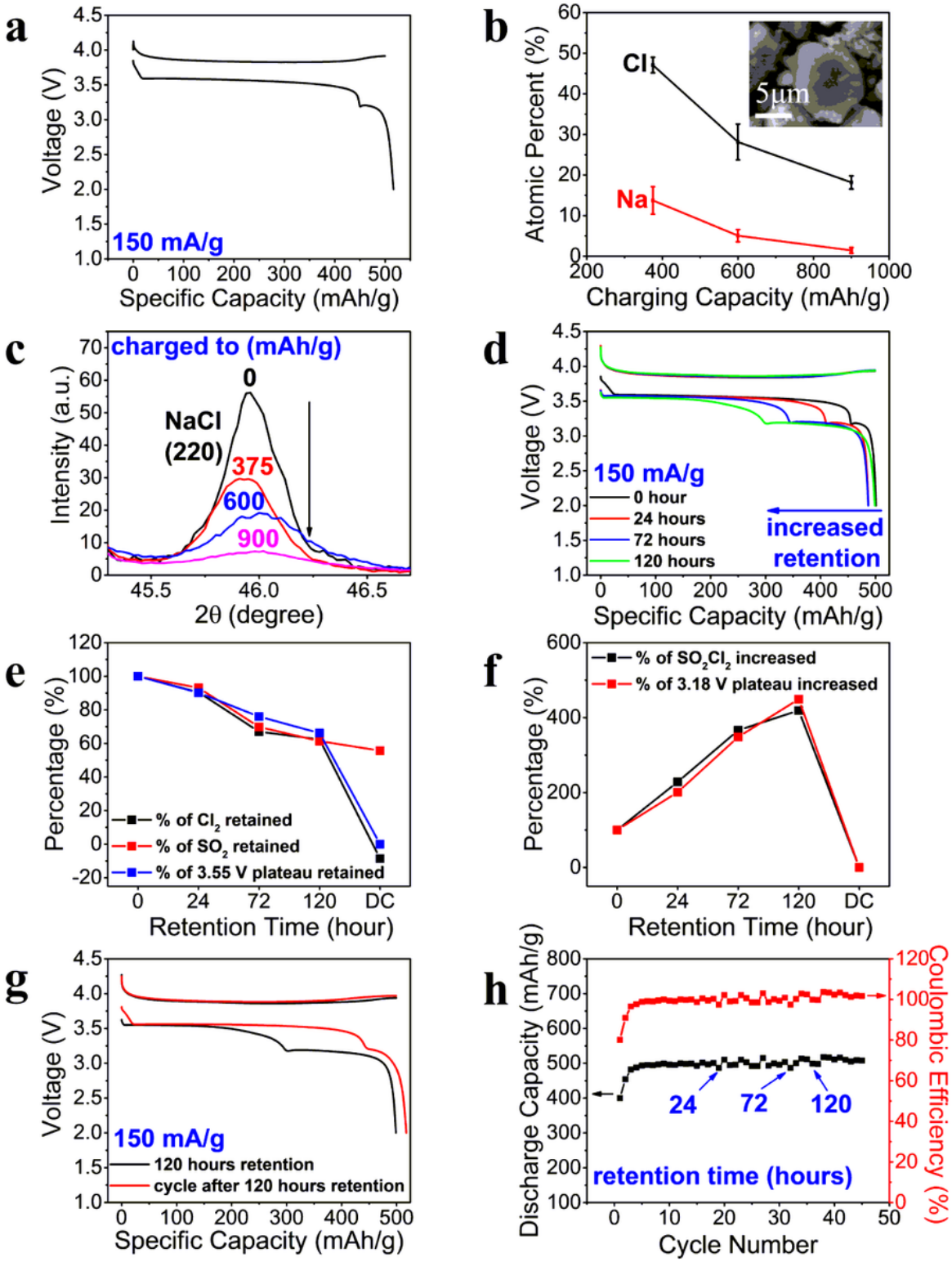

Figure 2

Rechargeable Na/Cl battery at different battery states through cycling. a, Charge – discharge curve of the battery at 500 mAh/g (150 mA/g). b, Atomic percentages of Na and Cl from XPS Survey spectra recorded on the aCNS cathode after the battery was charged to different capacities (inset: SEM imaging of the

cathode charged to 600 mAh/g with most of the NaCl removed). c, XRD spectra (normalized to Ni current collector) of aCNS cathodes showing evolution of the (220) diffraction peak of NaCl coating on the cathode when batteries in discharged state were charged to various capacities. NaCl was increasingly oxidized/removed from the cathode. d, Charge – discharge curve of a Na/Cl battery, with the discharge curves recorded after the battery was held at open circuit for different retention times in fully charged state. (e, f), Percentage changes for the parameters indicated versus battery retention time in open-circuit charged state for 0 hour, 24 hours, 72 hours and 120 hours before discharging. g, Charge – discharge curves (red) of a Na/Cl battery recorded after discharging the battery (black) post 120 hours retention in charged state. h, cycling performance of the Na/Cl battery with different retention cycles at 500 mAh/g (150 mA/g).

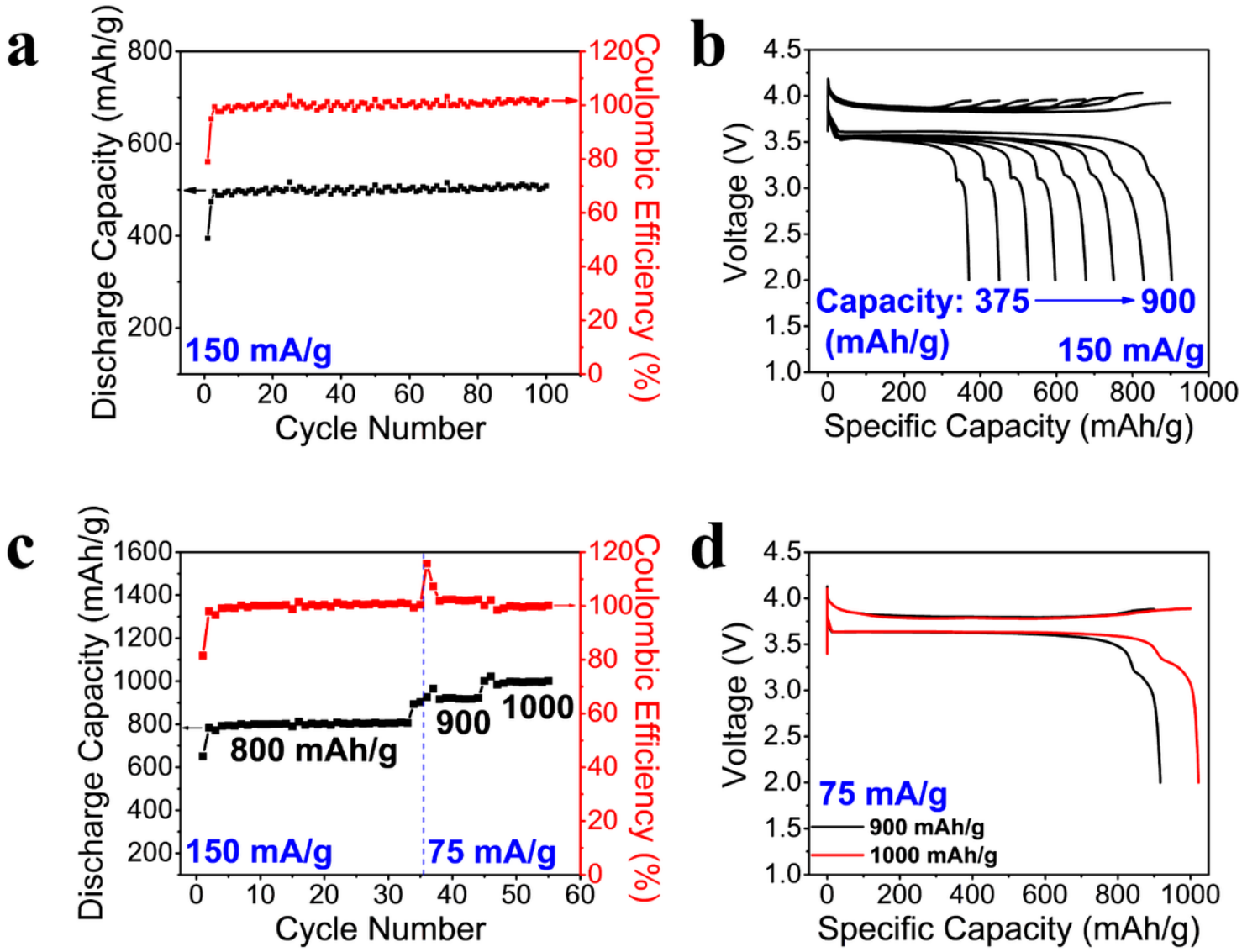

Figure 3

Cycling performance of Na/Cl battery at different capacities a, Cycling performance of a Na/Cl battery as the charging capacity was set to 500 mAh/g (150 mA/g). b, Charge – discharge curves of a Na/Cl battery

when the charging capacity was varied to range from 375 mAh/g – 900 mAh/g in step of 75 mAh/g (150 mA/g). c, Cycling performance of a Na/Cl battery when the charging capacity was from 800 mAh/g – 1000 mAh/g at currents of 150 mA/g and 75 mA/g. d, Charge – discharge curves of the Na/Cl battery at 900 mAh/g and 1000 mAh/g capacities (75 mA/g).

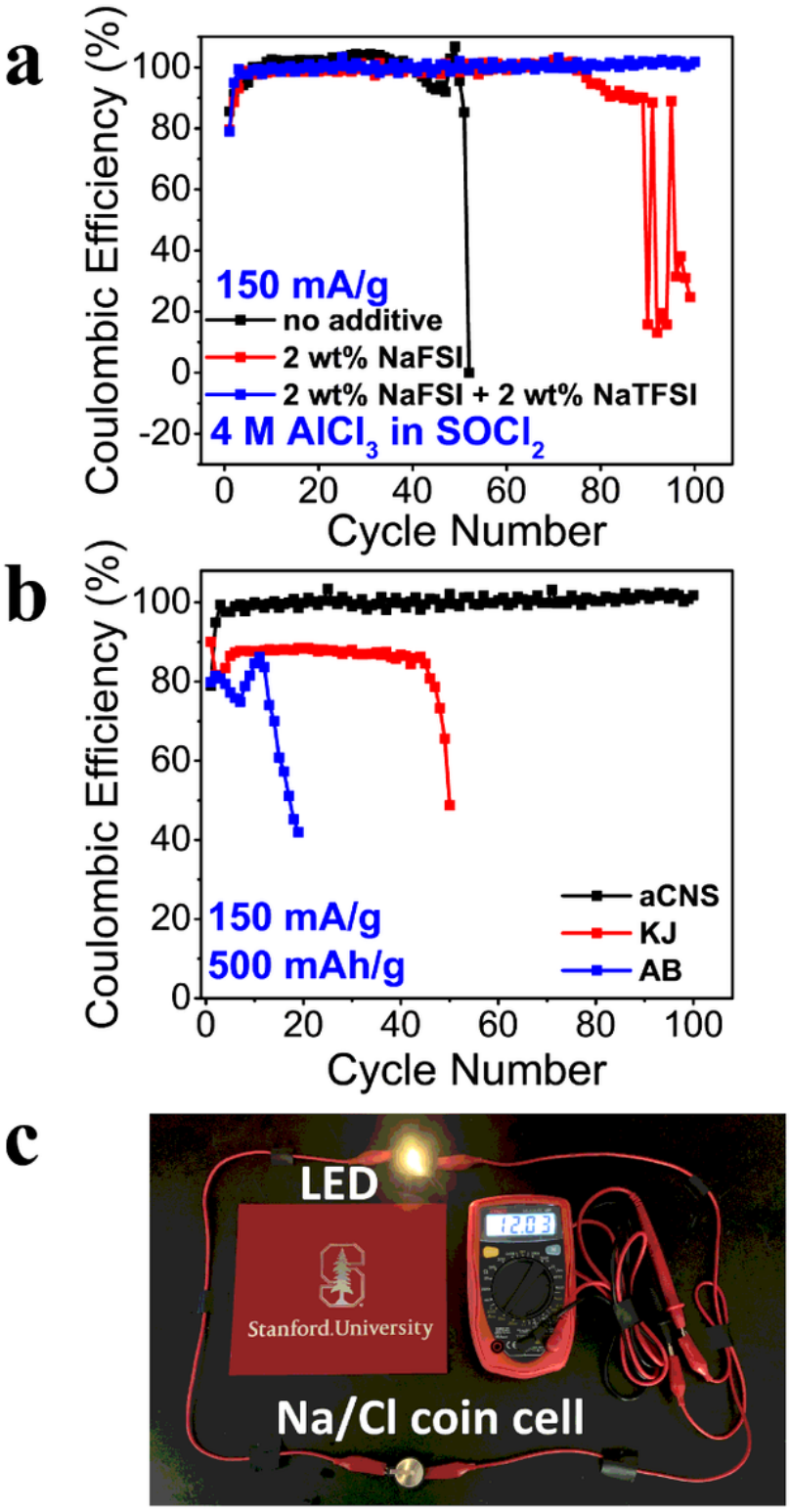

Figure 4

Importance of stable SEI on sodium anode and novel carbon cathode for Na/Cl battery. a, Coulombic efficiency comparison over cycling in 4 M AlCl3 in SOCl2 electrolytes with different additives indicated. The cycling capacity was 500 mAh/g (150 mA/g). b, Coulombic efficiency comparison over cycling for Na/Cl batteries using different carbon materials as the positive electrode. AB was commercially available Soltex, Acetylene Black 50%-01 and KJ was commercially available Ketjenblack EC-600JD. c, Lighting up an LED light using a Na/Cl battery coin cell at a 12.03 mA (4.57 mA/cm2 Na, 1563.35 mA/g aCNS) current. Coin cell is 20 mm in diameter and 3.2 mm in thickness.

Supplementary Files

This is a list of supplementary files associated with this preprint. Click to download.

- SI.docx
- ExtendedData.docx